Multi-Revolution Perturbed Lambert's Problem

Roberto Armellin * and David Gondelach†
University of Surrey, Guildford, Surrey, GU2 7XH, United Kingdom

Juan Felix San Juan‡
Universidad de La Rioja, Logroño, La Rioja, 26006, Spain

The solution of multiple-revolution perturbed Lambert problems is a challenging task due to the high sensitivity of the final state to variations of the initial velocity. In this work two different solvers based on high order Taylor expansions and an analytical solution of the J_2 problem are presented. In addition, an iteration-less procedure is developed to refine the solutions in a dynamical model that includes $J2 - J4$ perturbations. The properties of the proposed approached are tested against transfers with hundreds of revolutions including those required to solve the Global Trajectory Optimisation Competition 9.

I. Introduction

The Lambert problem is one of the most extensively studied problems in astrodynamics as its solution is a building block for many problems, including interplanetary transfer optimization, rendezvous missions design, and orbit determination for radar observations. Although this problem was solved more than 200 years ago [1], many researchers are still working on devising robust and efficient resolution procedures [2, 3]. In particular, when the transfer time is long, the Lambert's problem becomes a multiple-revolution Lambert's problem (MRLP) which has the additional difficulty of admitting many solutions associated with different number of revolutions. More specifically, there exists $2N_{max} + 1$ number of solutions to a MRLP, in which N_{max} is maximum number of revolutions compatible with the time-of-flight of interest [4].

The original formulation of the Lambert's problem is based on two-body dynamics. However, when the MRLP solutions are used to design missions around a planetary body or for orbit determination and data association problems, the effect of perturbations cannot be neglected. The perturbations, e.g. J_2 or atmospheric drag, can cause large violations of the terminal constraints, up to the point that classical Lambert's solutions fail to provide a good initial guess for the multiple-revolution perturbed Lambert's problem (MRPLP). Different methods have been proposed over the years to solve perturbed Lambert's problems. Engles and Junkins [5] proposed a variation-of-parameter approach combined with Kustaanheimo-Stiefl (KS) transformation to algebraically solve the J_2 perturbed problem. Bai and Junkins [6] proposed a modified Chebyshev-Picard iteration (MCPI) method for the solution of two-point boundary values problems, which was later regularized by Woollands et al. [7] using the KT time transformation. Der [8] developed a solver based on Vinti's approximation. However, these approaches are not suitable for cases with many revolutions, due to the fact that the initial Keplerian guess for the velocity is not close to the perturbed one.

More recently, Yang et al. [9] developed a homotopic approach suitable for solving the MRPLP, which they applied to the design of rendezvous missions around Mars. This approach employs a homotopy on the residuals. For each of the multiple solutions of the MRLP a sequence of MRPLP is solved for decreasing values of the homotopic parameter. Only when this parameter reaches zero the MRPLP is fully solved. Remarkably transfers with more than one thousand revolutions were presented, although limited details on how to define the continuation path were provided. Another solver suitable for MRPLP was published recently by Woollands et al. [10]. This method combines the MCPI method with the method of particular solution and has the favorable property of not requiring the computation of the state transition matrix. However, its performance was assessed with transfers with a limited number of revolutions.

In this work we present two MRPLP solvers based on the high order expansion of the flow enabled by Differential Algebra (DA) [11]. The first solver is suitable for solving a MRPLP when a Keplerian solution is available and is based on the application of homotopy on the perturbation. When the homotopic parameter ϵ is zero the problem is Keplerian, for which a solution is available. DA is used to expand the residuals at high order with respect to ϵ, and a continuation path is defined such that when $\epsilon = 1$ the MRPLP is solved. Using high order expansions brings the advantage that a)

*Senior Lecturer, Surrey Space Centre, BA Building
†PhD candidate, Surrey Space Centre, BA Building
‡Associate Professor, Departamento de Matemáticas y Computación, Edificio CCT

the continuation path can be defined in an automatic way based on an estimate of the truncation error of the Taylor expansion [12] and b) the number of required continuation steps is limited. The main limitation of this approach is that the first guess must be a solution of the Keplerian problem. However, there are cases in which using a Keplerian guess results in solutions with high Δv. This is particularly a drawback for cases in which the perturbations could be effectively used to reduce the mission Δv. A second approach solves this issue. Here DA is exploited to expand to high order the problem residuals with respect to the initial velocity. A nonlinear solver is then used to compute the zeros of the polynomial representation of the residuals, and the process is repeated until the polynomial representation is accurate enough to deliver low residuals for the MRPLP.

In both the proposed approaches, a first order analytical solution of the J_2 problem is used to reduce the computation time. The analytical solution is based on Brouwer's theory written in polar-nodal variables [13] that typically provides kilometer-level accuracy for solutions involving up to several hundred revolutions. For cases in which higher accuracy is demanded a single high order DA-based shooting iteration is applied to further refine the solution. Remarkably this refinement step can be exploited to include other relevant perturbations previously neglected, e.g. higher order geopotential harmonics. The availability of the high order expansion of the solution of the two-point boundary value problem can be efficiently used to study the optimality of the transfer based on the study of evolution of the primer vector [14].

In the following, the Differential Algebra techniques and the applied dynamical models are discussed. After that, the two novel Lambert solvers are introduced as well as the refinement technique and the use of primer vector theory to study the optimality of the transfers. Finally, the solvers are tested for different MRPLPs, including those required to solve the Global Trajectory Optimisation Competition 9 (GTOC9)*.

II. Differential Algebra tools

DA supplies the tools to compute the derivatives of functions within a computer environment [15]. More specifically, by substituting the classical implementation of real algebra with the implementation of a new algebra of Taylor polynomials, any deterministic function f of v variables that is C^{k+1} in the domain of interest $[-1, 1]^v$ (these properties are assumed to hold for any function dealt with in this work) is expanded into its Taylor polynomial up to an arbitrary order k with limited computational effort. In addition to basic algebraic operations, operations for differentiation and integration can be easily introduced in the algebra, thusly finalizing the definition of the differential algebraic structure of DA [16, 17]. Similarly to algorithms for floating point arithmetic, various algorithms were introduced in DA, including methods to perform composition of functions, to invert them, to solve nonlinear systems explicitly, and to treat common elementary functions [18]. The DA used for the computations in this work was implemented in the softwares COSY INFINITY [19] and DACE [20].

A. Expansion of the solution of ordinary differential equations

An important application of DA is the automatic computation of the high order Taylor expansion of the solution of ordinary differential equations (ODE) with respect to either the initial conditions or any parameter of the dynamics [21, 22]. This can be achieved by replacing the classical floating point operations of the numerical integration scheme, including the evaluation of the right hand side, by the corresponding DA-based operations. This way, starting from the DA representation of the initial condition x_0, the DA-based ODE integration supplies the Taylor expansion of the flow in x_0 at all the integration steps, up to any final time t_f. Any explicit ODE integration scheme can be adapted to work in the DA framework in a straightforward way. For the numerical integrations presented in this paper, a DA version of a 7/8 Dormand-Prince (8-th order solution for propagation, 7-th order solution for step size control) Runge-Kutta scheme is used. The main advantage of the DA-based approach is that there is no need to write and integrate variational equations to obtain high order expansions of the flow. It is therefore independent on the particular right hand side of the ODE and the method is quite efficient in terms of computational cost.

B. Estimation of truncation error

The selection of the expansion order is a crucial issue when using high order Taylor representations. The order must be selected so that the truncation error of the Taylor representation of the function of interest $\mathcal{T}_f$ is lower than a threshold that is deemed appropriate for the problem at hand.

*https://sophia.estec.esa.int/gtoc_portal/?page_id=814

A coefficient-based method to estimate the truncation error is used in this work. The method estimates the size of the $k+1$ order terms, of the Taylor polynomial, $t(k+1)$, based on an exponential fit of the size of all the known non-zero coefficients up to order k. The value of $t(k+1)$ is used to estimate the size S_{k+1} of the truncated order $k+1$ of $\mathcal{T}_f$. This value is representative of the accuracy of the Taylor approximation of order k in the domain of interest. Thus, for a given problem, the order k to be used for the DA computations is selected so that S_{k+1} is lower than a prescribed tolerance. It has to be remarked that this approach gives an accurate estimate of the truncation error when a sufficient number of coefficients is available for the fit, i.e. for a sufficiently high value of k (say above 3). For more details the reader is referred to [12].

III. Dynamics

The most complete dynamical model considered in this work is described by

$$\begin{cases} \dot{x} = v_x, \dot{y} = v_y, \dot{z} = v_z \\ \dot{v_x} = -\frac{\mu x}{r^3} + \frac{3\mu J_2 R_e^2}{2r^5}(\frac{5z^2}{r^2} - 1)x + \frac{5\mu J_3 R_e^3 xz}{2r^7}(\frac{7z^2}{r^2} - 3) + \frac{15\mu J_4 R_e^4 x}{8r^7}(1 - \frac{14z^2}{r^2} + \frac{21z^4}{r^4}) \\ \dot{v_y} = -\frac{\mu y}{r^3} + \frac{3\mu J_2 R_e^2}{2r^5}(\frac{5z^2}{r^2} - 1)y + \frac{5\mu J_3 R_e^3 yz}{2r^7}(\frac{7z^2}{r^2} - 3) + \frac{15\mu J_4 R_e^4 y}{8r^7}(1 - \frac{14z^2}{r^2} + \frac{21z^4}{r^4}) \\ \dot{v_z} = -\frac{\mu z}{r^3} + \frac{3\mu J_2 R_e^2}{2r^5}(\frac{5z^2}{r^2} - 3)z + \frac{5\mu J_3 R_e^3}{2r^5}(\frac{3}{5} - \frac{6z^2}{r^2} + \frac{7z^4}{r^4}) + \frac{15\mu J_4 R_e^4 z}{8r^7}(5 - \frac{70z^2}{3r^2} + \frac{21z^4}{r^4}) \end{cases} \tag{1}$$

in which $\boldsymbol{r} = [x, y, z]^T$ and $\boldsymbol{v} = [v_x, v_y, v_z]^T$ are the spacecraft position and velocity vector; μ, R_e, and J_i are the gravitational parameter, the mean equatorial radius, and the i-th zonal harmonic coefficient of the Earth. The numerical integration of Eq. (1) is time consuming when long transfer time are considered, thus its use in the solution of MRPLP is impractical. For this reason, in the proposed solvers, the numerical propagation of Eq. (1) is replaced by an analytical solution of the J_2 problem, described in Section A. The solution obtained with the analytical propagator is then refined numerically by exploiting DA tools for expanding the flow of ODE. Note that, as for the Earth the contribution due to J_2 is an order of magnitude larger than that of other harmonics, the numerical refinement of the solution will not require iterations. In addition, it is worth underlining that the approach described in the paper is valid for any perturbed dynamical model in which J_2 is the dominant perturbation, and thus we are not restricted to the dynamical system described in Eq. (1).

A. Analytical solution of J_2 problem

The Hamiltonian for the J_2 problem in the artificial satellite theory is given in Delaunay's variables (l, g, h, L, G, H)[†] by

$$\mathcal{H} = \mathcal{H}_0 + \epsilon \mathcal{H}_1 \tag{2}$$

where

$$\begin{aligned} \mathcal{H}_0 &= -\frac{\mu^2}{2L^2}, \\ \mathcal{H}_1 &= \frac{\mu}{r}\left(\frac{R_e}{r}\right)^2 P_2\left(s\,\sin(f+g)\right), \end{aligned}$$

$\epsilon = J_2$, P_2 is the Legendre polynomial of degree 2, r is the radial distance, f is the true anomaly and s is the sine of the inclination i.

This two-degree-of-freedom degenerate Hamiltonian is non-integrable. However, by applying the Lie-Deprit method, an approximate first-order closed-form analytical solution can be obtained. Using MathATESAT [23], the short-period terms, caused by the true anomaly, are removed by applying the Lie transform $\varphi : (l, g, h, L, G, H) \rightarrow (l', g', h', L', G', H')$, so-called Delaunay Normalization [24], which at zero and first orders give

$$\mathcal{K}_0 = \mathcal{H}_0 \tag{3}$$

$$\mathcal{K}_1 = \mathcal{H}_1 - \frac{\mu^2}{L'^3}\frac{\partial \mathcal{W}}{\partial l'} \tag{4}$$

[†]The Delaunay variables relate to the Keplerian orbital elements as follows: $l = M$, $g = \omega$, $h = \Omega$, $L = \sqrt{\mu a}$, $G = L\sqrt{1-e^2}$, $H = G\cos i$)

The Lie-Deprit method solves Eq. (4) by choosing the form of the transformed Hamiltonian $\mathcal{K}$; the Delaunay Normalization takes the Hamiltonian as the average over the fastest angle l':

$$\mathcal{K}_1 = \frac{3R_e^2\mu^4 s'^2}{4L'^6\eta'^3} - \frac{R_e^2\mu^4}{2L'^6\eta'^3} \tag{5}$$

and then $\mathcal{W}_1$ is computed as

$$\begin{aligned} \mathcal{W}_1 &= \frac{L'^3}{\mu^2}\int (\mathcal{H}_1 - \mathcal{K}_1)dl \\ &= \frac{R_e^2\mu^2}{2\eta'^3 L'^3}\left[\left(\frac{3s'^2}{2} - 1\right)(\phi' + e'\sin f') - \frac{3}{4}e's'^2\sin(f' + 2g') \right. \\ &\quad \left. -\frac{3}{4}s'^2\sin(2f' + 2g') - \frac{1}{4}e's'^2\sin(3f' + 2g')\right] \end{aligned} \tag{6}$$

where $\eta' = \sqrt{1 - e'^2}$ and $\phi' = f' - l'$.

Hence, up to the first order, the transformed Hamiltonian is given by:

$$\mathcal{K} = -\frac{\mu^2}{2L'^2} + \epsilon\left(\frac{3R_e^2\mu^4 s'^2}{4L'^6\eta'^3} - \frac{R_e^2\mu^4}{2L'^6\eta'^3}\right) \tag{7}$$

This Hamiltonian only depends on the momenta L', G' and H', and so the equations of motion are obtained as

$$\begin{aligned} \frac{\mathrm{d}l'}{\mathrm{d}t} = \frac{\partial\mathcal{K}}{\partial L'} &= \frac{\mu^2}{L'^3} + \epsilon\left(\frac{3R_e^2\mu^4}{2L'^7\eta'^3} - \frac{9R_e^2\mu^4 s'^2}{4L'^7\eta'^3}\right) \\ \frac{\mathrm{d}g'}{\mathrm{d}t} = \frac{\partial\mathcal{K}}{\partial G'} &= \epsilon\left(\frac{3R_e^2\mu^4}{L'^7\eta'^4} - \frac{15R_e^2\mu^4 s'^2}{4L'^7\eta'^4}\right) \\ \frac{\mathrm{d}h'}{\mathrm{d}t} = \frac{\partial\mathcal{K}}{\partial G'} &= -\epsilon\frac{3R_e^2\mu^4 c'}{2L'^7\eta'^4} \\ \frac{\mathrm{d}L'}{\mathrm{d}t} = \frac{\mathrm{d}G'}{\mathrm{d}t} &= \frac{\mathrm{d}H'}{\mathrm{d}t} = 0 \end{aligned} \tag{8}$$

By integrating Eq. (8) we can directly obtain that the values of the momenta L', G' and H' are constants, whereas the variables l', g' and h' are

$$\begin{aligned} l' &= \left[\frac{\mu^2}{L'^3} + \epsilon\left(\frac{3R_e^2\mu^4}{2L'^7\eta'^3} - \frac{9R_e^2\mu^4 s'^2}{4L'^7\eta'^3}\right)\right](t - t_0) + l'_0 \\ g' &= \left[\epsilon\left(\frac{3R_e^2\mu^4}{L'^7\eta'^4} - \frac{15R_e^2\mu^4 s'^2}{4L'^7\eta'^4}\right)\right](t - t_0) + g'_0 \\ h' &= \left[-\epsilon\frac{3R_e^2\mu^4 c'}{2L'^7\eta'^4}\right](t - t_0) + h'_0 \end{aligned} \tag{9}$$

where l'_0, g'_0, h'_0, L'_0, G'_0, H'_0 are the transformed initial conditions l_0, g_0, h_0, L_0, G_0, H_0 at the epoch t_0.

This first-order analytical solution is concluded by computing the transformation equation in a non-singular form [13, 25]. Using polar-nodal variables $(r, \theta, \nu, R, \Theta, N)$[‡], Eq. (6) yields

$$\mathcal{W}_1 = \frac{R_e^2}{4p'}\left[\left(3s'^2 - 2\right)\left(\frac{\Theta'\phi'}{p'} + R'\right) + s'^2\Theta'\left(\frac{1}{2p'} + \frac{2}{r'}\right)\sin 2\theta' + s'^2R'\cos 2\theta'\right]$$

[‡]The polar-nodal variables relate to radial distance r and orbital elements as follows: $\theta = \omega + f$, $\nu = \Omega$, $R = \dot{r}$, $\Theta = \sqrt{\mu a(1 - e^2)}$, $N = \Theta\cos i$

Finally, the transformation equations are obtained from the expression

$$\delta = \delta' + \{\delta', \mathcal{W}_1\}$$

where $\delta \in (r, \theta, \nu, R, \Theta, N)$ and $\{\,, \mathcal{W}_1\}$ represents a differential operator so-called Poisson bracket. The expressions of $\{\delta', \mathcal{W}_1\}$ are given in the Appendix whereas the relations between the old and new variables are obtained by replacing prime by non-prime variables respectively in the expression

$$\delta' = \delta + \{\delta, \mathcal{U}_1\}$$

where $\mathcal{U}_1 = -\mathcal{W}_1$.

IV. Solution of multiple-revolution perturbed Lambert's problem

In Lambert's problem, the initial position, $\boldsymbol{r}_i$, final position, $\boldsymbol{r}_f$, and the time-of-flight between the two positions are given. Solving Lambert's problem defines the orbit that connects the two position vectors in the specified time-of-flight $\Delta t = t_f - t_i$, allowing the calculation of the velocities at the initial and final positions of the connecting orbit, referred to as $\boldsymbol{v}_i$ and $\boldsymbol{v}_f$. The Lambert problem is frequently used in trajectory design to compute the transfer arc between a departing and arrival orbit, associated with a departing and an arrival body (e.g. two celestial bodies for interplanetary transfers or two spacecraft for Earth orbiting missions). In these cases $\boldsymbol{r}_1$ and $\boldsymbol{v}_1$ are the position and velocity vectors of the first body at t_i, and $\boldsymbol{r}_2$ and $\boldsymbol{v}_2$ are the position and velocity vectors of the second body at t_f, see Figure 1. The total cost of the transfer is the impulse to inject the spacecraft on the transfer arc $\Delta v_1 = ||\boldsymbol{v}_i - \boldsymbol{v}_1||$ and the impulse for the rendezvous $\Delta v_2 = ||\boldsymbol{v}_2 - \boldsymbol{v}_f||$. The classical formulation of the Lambert problem considers Keplerian motion. In such case, there is no need to numerically propagate the transfer trajectory and the problem reduces to the numerical solution of a nonlinear equation. When the time-of-flight is sufficiently long multiple solutions appear associated with different number of revolutions. The maximum number of revolutions is $N_{max} = \text{floor}\left(\frac{\Delta t}{2\pi}\sqrt{\frac{\mu}{a_m^3}}\right)$, in which μ is the gravitational parameter and $a_m = \frac{1}{4}\left(r_1 + r_2 + ||\boldsymbol{r}_1 - \boldsymbol{r}_2||\right)$. There are two solutions for each revolution number, thus there exists $2N_{max} + 1$ number of solutions to a MRLP.

When perturbations are included, Lambert's problem becomes more difficult to solve for two main reasons. Firstly, for long time-of-flights the solution of the MRLP may not provide a good guess for the perturbed problem. In particular, the perturbation due to J_2 is the largest for most of the orbital regimes around the Earth. The effect of the J_2 perturbation can be strong and as a result the solution of the MRLP may produce high residuals and shooting methods may diverge. Secondly, exact analytical solutions are not available for perturbed dynamics and thus one either needs to use approximate solutions or time-consuming numerical propagations. The first problem is the most challenging one, as it requires the implementation of ad hoc strategies to assure convergence. Two different solvers are proposed to deal with this problem, one based on a homotopy approach on the perturbation (see Section IVA) and one on the repetitive solution of a surrogate problem, as described in Section IVB. The second issue is tackled here, in a first instance, by substituting the numerical integration of Eq. (1) by the analytical solution of the J_2 problem described in Section IIIA. The approximate solution is then refined numerically in the full dynamical model taking advantage of the high order expansion of the flow enabled by DA, as described in Section IVC. Finally, the application of primer vector theory (Section IVD) to study the optimality of a transfer is discussed together with additional algorithms to expand the solution of the MRPLP (Section IVE).

A. J_2-homotopy solver

Suppose that $\boldsymbol{v}_i^K$ is the solution of the MRLP, i.e. the initial velocity that solves the Lambert problem with Keplerian dynamics. Using $\boldsymbol{v}_i^K$ as initial velocity in the perturbed problem results in a final residual $\Delta\boldsymbol{r}_2 = \boldsymbol{r}_f^{J_2} - \boldsymbol{r}_2 \neq 0$. The objective is to find $\boldsymbol{v}_i^{J_2}$, the solution of the J_2 Lambert's problem, i.e. the velocity vector that connects $\boldsymbol{r}_1$ to $\boldsymbol{r}_2$ in Δt when the J_2 harmonic is accounted for.

In the following we present a homotopic approach to robustly solve this problem. Differently from a previously proposed approach [9], the homotopy is not applied to the residuals, but to the perturbation itself as typically done in perturbation theory.

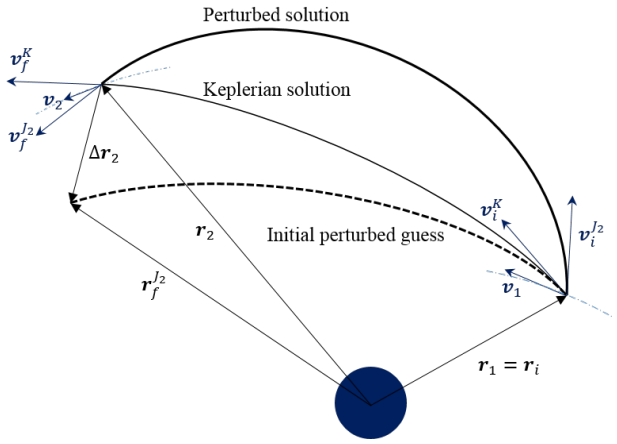

Fig. 1 Schematic drawing of perturbed Lambert problem.

Consider the perturbed dynamics

$$\begin{cases} \dot{\boldsymbol{r}} &= \boldsymbol{v} \\ \dot{\boldsymbol{v}} &= \boldsymbol{f}^K(\boldsymbol{r},\boldsymbol{v},\boldsymbol{p},t) + \epsilon \boldsymbol{f}^{J_2}(\boldsymbol{r},\boldsymbol{v},\boldsymbol{p},t) \end{cases} \tag{10}$$

in which $\boldsymbol{p}$ is a generic vector of parameters, and the homotopic parameter ϵ is a DA variable. The forward integration of Eq. (10) with initial velocity $\boldsymbol{v}_i$ initialized as a DA vector about the Keplerian solution $\boldsymbol{v}_i^K$ provides the Taylor map of the final state

$$\boldsymbol{r}_f^{\epsilon J_2} = \mathcal{T}_{\boldsymbol{r}_f}(\boldsymbol{v}_i, \epsilon) \tag{11}$$

The Taylor representation of the residuals is readily available by

$$\Delta\boldsymbol{r}_2 = \boldsymbol{r}_f^{\epsilon J_2} - \boldsymbol{r}_2 = \mathcal{T}_{\Delta\boldsymbol{r}_2}(\boldsymbol{v}_i, \epsilon) \tag{12}$$

This polynomial map tells us how the final residuals change when the initial velocity and the homotopic parameter changed. The map is partially inverted using DA tools to obtain the Taylor expansion that maps $\boldsymbol{\Delta r}_2$ and ϵ to the initial velocity:

$$\boldsymbol{v}_i = \mathcal{T}_{\boldsymbol{v}_i}(\boldsymbol{\Delta r}_2, \epsilon). \tag{13}$$

When evaluated in $\boldsymbol{\Delta r}_2 = 0$, map (13) provides the initial velocity vector that solves the MRPLP for different values of ϵ. For $\epsilon = 1$ the correction for the full J_2 problem is achieved,

$$\boldsymbol{v}_i^{J_2} = \mathcal{T}_{\boldsymbol{v}_i}(\boldsymbol{\Delta r}_2 = 0, \epsilon = 1). \tag{14}$$

However, directly computing $\boldsymbol{v}_i^{J_2}$ using Eq. (14) may result in large residuals for long time-of-flight due to truncation errors of the Taylor approximation. Therefore, the initial velocity vector is evaluated for increasing values of $\epsilon \in [0, 1]$, i.e. for a dynamical system that progressively approaches the full J_2 problem.

The determination of the proper continuation path, i.e. the proper increase of ϵ, is one main difficulties in homotopy approaches. In our approach the continuation path is computed automatically by estimating the truncation error of Eq. (13) with respect to ϵ, and by selecting its increase such that a demanded accuracy on the velocity vector is met. An accuracy of $1e-6$ km/s was chosen for the test cases presented in this paper.

B. J_2-map Lambert's solver

The continuation method described in the previous section is based on the assumption that a Keplerian first guess is available and that this is a good guess for the J_2 Lambert's problem. However, this is not always the case in particular when long flight times are considered and the effect of J_2 can be exploited to reduce the Δv significantly. In these cases a better first guess may be available, e.g. the velocity of the departing body, that is however not the solution of two-body Lambert's problem. In such conditions the homotopic approach described in Section IVA may fail to converge due to the high initial values of the residuals. The following solver is proposed to deal with such cases.

The algorithm starts by initializing the departure velocity as a DA variable about an initial guess for $\boldsymbol{v}_i^g$. The forward propagation of the DA initial state provides the Taylor expansion of final state at t_f

$$\boldsymbol{r}_f^{J_2} = \mathcal{T}_{\boldsymbol{r}_f^{J_2}}(\boldsymbol{v}_i) \tag{15}$$

The residuals of the J_2 Lambert's problem are then expressed as a high order Taylor map by

$$\Delta\boldsymbol{r}_2 = \boldsymbol{r}_f^{J_2} - \boldsymbol{r}_2 = \mathcal{T}_{\Delta\boldsymbol{r}_2}(\boldsymbol{v}_i). \tag{16}$$

A nonlinear solver (e.g. the *fzero* function of MATLAB [26]) is then used to compute the velocity vector $\boldsymbol{v}_i^j$ for which the Taylor representation of the residual function (Eq. (16)) is zero, i.e.

$$\mathcal{T}_{\Delta\boldsymbol{r}_2}(\boldsymbol{v}_i^j) = 0 \tag{17}$$

It should however be noted that $\boldsymbol{v}_i^j$ is the solution of an approximated problem (i.e. the Taylor expansion of the residuals) and, for large initial residuals, will not provide an accurate solution. The accuracy of the solution can be checked by computing the new defects using $\boldsymbol{v}_i^j$ as new guess, and if they do not meet the prescribed accuracy, the procedure is repeated and a new departure velocity is computed. The iterations stops when the computed initial velocity solves the J_2 Lambert's problem with the demanded accuracy, thus delivering $\boldsymbol{v}_i^{J_2}$. It is important to notice that this approach is practical from a computational standpoint because 1) the analytical solution of the J_2 problem is used and 2) each iteration consists only of finding the numerical solution of three polynomial equations. Furthermore, it is worth observing that the J_2-map Lambert's solver can also be used when the first guess is the solution of the MRLP and that, in this case, a continuation in the perturbation (as described in Section IVA) could be adopted to improve robustness.

C. Iteration-less refinement

Both the homotopic J_2 Lambert's solver and the J_2-map Lambert's solver use the analytical solution of J_2 problem to limit the computational time. As a result, if Eq. (1) are propagated numerically with the computed approximated solution, the residuals on the final position won't be zero (they are typically of few kilometers for transfer times of several days). Thus, an algorithm to refine the solution in the full dynamical model is needed.

For the sake of generality, consider the case in which $\boldsymbol{v}_i^A$, an approximate solution of the perturbed Lambert problem, is available. The objective is to solve Lambert's problem for the full dynamical model

$$\begin{cases} \dot{\boldsymbol{r}} &= \boldsymbol{v} \\ \dot{\boldsymbol{v}} &= \boldsymbol{f}^F(\boldsymbol{r}, \boldsymbol{v}, \boldsymbol{p}, t) \end{cases} \tag{18}$$

in which $\boldsymbol{f}^F(\boldsymbol{r}, \boldsymbol{v}, \boldsymbol{p}, t)$ can include additional perturbations not considered when computing for the approximate solution. In this work the full dynamical model is given by Eq. (1). The goal is then to compute the initial velocity $\boldsymbol{v}_i^F$ such that the forward propagation of the full dynamics for Δt results in $\boldsymbol{r}_f^F = \boldsymbol{r}_2$ within a given tolerance.

The forward propagation of Eq. (18) with initial conditions $(\boldsymbol{r}_1, \boldsymbol{v}_i^A)$ results in a residual $\Delta\boldsymbol{r}_2 = \boldsymbol{r}_f^F - \boldsymbol{r}_2 \neq \boldsymbol{0}$. However, if the additional perturbations are small and/or Δt is short the residual $\Delta\boldsymbol{r}_f$ is small. In that case, high order Taylor expansions provided by DA can be used to compute the correction to the initial velocity such that $\Delta\boldsymbol{r}_f = 0$ without the need of iterations. The procedure can be summarized as follows.

The initial velocity is initialized as a DA vector about $\boldsymbol{v}_i^A$ and the dynamics, Eq. (18), are propagated forward for Δt using a DA propagator, delivering the expansion of the final state with respect to the initial velocity vector

$$\boldsymbol{r}_f^F = \mathcal{T}_{\boldsymbol{r}_f^F}(\boldsymbol{v}_i). \tag{19}$$

In Eq. (19), $\mathcal{T}_{\boldsymbol{r}_f^F}(\boldsymbol{v}_i)$ is a high order Taylor polynomial that maps a variation in the initial velocity to the final time in the full dynamical model. The Taylor representation of the residual is computed by subtracting $\boldsymbol{r}_2$ from Eq. (19),

$$\Delta\boldsymbol{r}_2 = \boldsymbol{r}_f^F - \boldsymbol{r}_2 = \mathcal{T}_{\Delta\boldsymbol{r}_2}(\boldsymbol{v}_i). \tag{20}$$

Eq. (20) can be inverted with DA tools, delivering

$$\boldsymbol{v}_i = \mathcal{T}_{\boldsymbol{v}_i}(\boldsymbol{\Delta r}_2). \tag{21}$$

An approximated solution of the problem is then obtained by evaluating map (21) in $\Delta \boldsymbol{r}_2 = 0$,

$$\boldsymbol{v}_i^F = \mathcal{T}_{\boldsymbol{v}_i}(\Delta \boldsymbol{r}_2 = 0). \tag{22}$$

The described procedure is nothing else than a high order implementation of a shooting method [21]. When $\boldsymbol{v}_i^A$ is sufficiently close to $\boldsymbol{v}_i^F$ then the velocity correction can be obtained with a single iteration. This is the case when, for example, the approximate dynamical model already includes the J_2 perturbation and when the effect of other perturbations included in $\boldsymbol{f}^F$ is small. The accuracy of the solution can be checked by computing the residuals with a forward propagation of the updated initial condition (22).

D. Primer vector analysis

Primer vector theory can be used to analyze if an orbital transfer is optimal. The term primer vector was introduced by Derek F. Lawden [27] and represents the adjoint vector for velocity. As shown by Lawden, the following four necessary conditions must be satisfied in order for an impulsive orbital transfer to be locally optimal:

1) the primer vector $\boldsymbol{p}$ and its first derivative $\dot{\boldsymbol{p}}$ are everywhere continuous;
2) when a velocity impulse $\Delta \boldsymbol{v}_k$ occurs at time t_k, the primer is a unit vector aligned with the impulse and has unit magnitude: $\boldsymbol{p}(t_k) = \frac{\Delta \boldsymbol{v}_k}{\Delta v_k}$;
3) the magnitude of the primer vector may not exceed unity on a coasting arc: $p(t) \leq 1$;
4) at all interior impulses (with the exception of the initial or final ones) $\boldsymbol{p}(t_k) \cdot \dot{\boldsymbol{p}}(t_k) = 0$, i.e. $\frac{\mathrm{d}p}{\mathrm{d}t}|_{t_k} = 0$.

For perturbations that depend only on the position vector (e.g. Earth's Geopotential and third body perturbation) it can be shown that the primer vector dynamics are defined by

$$\ddot{\boldsymbol{p}} = \frac{\partial f(\boldsymbol{r}, \boldsymbol{v}, t)}{\partial \boldsymbol{r}} \boldsymbol{p}. \tag{23}$$

As a result, the computation of the primer vector requires the solution of the boundary value problem defined by the dynamics

$$\begin{Bmatrix} \boldsymbol{p} \\ \dot{\boldsymbol{p}} \end{Bmatrix} = \Phi(t_i, t) \begin{Bmatrix} \boldsymbol{p}_i \\ \dot{\boldsymbol{p}}_i \end{Bmatrix} \tag{24}$$

in which $\Phi(t_i, t)$ is the state transition matrix (STM), and the boundary conditions

$$\begin{cases} \boldsymbol{p}_i = \frac{\Delta \boldsymbol{v}_1}{\Delta v_1} \\ \boldsymbol{p}_f = \frac{\Delta \boldsymbol{v}_2}{\Delta v_2}. \end{cases} \tag{25}$$

The initial value of the primer vector derivative $\dot{\boldsymbol{p}}_i$ is determined by

$$\dot{\boldsymbol{p}}_i = \Phi_{1,2}^{-1}(t_i, t_f) \left(\boldsymbol{p}_f - \Phi_{1,1}(t_i, t_f) \boldsymbol{p}_i \right) \tag{26}$$

in which $\Phi_{1,1}(t_i, t_f) = \frac{\partial \boldsymbol{r}_f}{\partial \boldsymbol{r}_i}$ and $\Phi_{1,2}(t_i, t_f) = \frac{\partial \boldsymbol{r}_f}{\partial \boldsymbol{v}_i}$.

The state transition matrix is analytically available for Keplerian motion, however numerical differentiation or calculus of variation are required for perturbed dynamics. The STM can be efficiently and accurately computed using DA by simply initializing the full initial state as a DA vector and performing the DA propagation at first order. With respect to the variational approach, DA allows us to avoid the analytical computation of the partial derivatives of the ODE's right-hand side and avoid the integration of a large system of ODEs. In addition, the DA approach allows us to compute the STM with the accuracy of the propagator, a result difficult to achieve with finite differences.

E. Expansion of the solution of the perturbed Lambert's problem

Prime vector theory provides a tool to understand whether a Lambert's arc is locally optimal. If p goes above one during the transfer a deep space or corrective maneuvres should be included such that the optimality conditions are met. To include deep-space maneuvers it is thus necessary to study how a perturbation of the position vector when $p_{max} > 1$ affects the total mission Δv. Although the study of the inclusion of deep space maneuvers is beyond the scope of this work in the following we provide a procedure to exploit DA computation to expand the solution of the perturbed Lambert problem with respect to perturbation in both the initial and final position vectors.

We start from the solution of the perturbed Lambert's problem, i.e. $\boldsymbol{v}_i$ such that $\boldsymbol{r}_f = \boldsymbol{r}_2$ and we initialize the initial state as DA vector. The initial state is propagated forward using the DA propagator obtaining

$$\begin{cases} \boldsymbol{r}_f &= \mathcal{T}_{\boldsymbol{r}_f}(\boldsymbol{r}_i, \boldsymbol{v}_i) \\ \boldsymbol{v}_f &= \mathcal{T}_{\boldsymbol{v}_f}(\boldsymbol{r}_i, \boldsymbol{v}_i). \end{cases} \tag{27}$$

The position component of map (27) can be inverted to deliver

$$\boldsymbol{v}_i = \mathcal{T}_{\boldsymbol{v}_i}(\boldsymbol{r}_i, \boldsymbol{r}_f) \tag{28}$$

Map (28) readily provides how a variation in both the initial and final position vectors affect the initial velocity. The effect on the final velocity $\boldsymbol{v}_f$ can be computed by polynomial composition, i.e. by substituting $\boldsymbol{v}_i = \mathcal{T}_{\boldsymbol{v}_i}(\boldsymbol{r}_i, \boldsymbol{r}_f)$ in the second row of Eq. (27), thus obtaining

$$\boldsymbol{v}_f = \mathcal{T}_{\boldsymbol{v}_f}(\boldsymbol{r}_i, \boldsymbol{r}_f). \tag{29}$$

Equations (28) and (29) can be used to study the insertion of corrective maneuvers on the total mission Δv, thus extending the linear theory of Jezewski [14] to arbitrary order.

V. Test cases

The algorithms presented in this paper were applied to design bi-impulsive transfers between synthetic space debris whose ephemerides were distributed by the Advanced Concepts Team of the European Space Agency in the frame of GTOC9. While the motion of the spacecraft is described by the full J_2 problem, the motion of the space debris is affected by J_2 only in an average way, i.e. the precession rates of the argument of perigee, ω, and right ascension of the ascending node, Ω, are given by

$$\begin{cases} \dot{\omega} &= \dfrac{3}{4} J_2 n \left(\dfrac{R_e}{a}\right)^2 \dfrac{5\cos^2 i - 1}{(1-e^2)^2} \\ \dot{\Omega} &= -\dfrac{3}{2} J_2 n \left(\dfrac{R_e}{a}\right)^2 \dfrac{\cos i}{(1-e^2)^2} \end{cases} \tag{30}$$

in which a, e, i, n are semi-major axis, eccentricity, inclination, and mean motion (all constant). All debris are in near-circular orbits between 600 and 900 km altitude with an inclination between 96 and 101 deg. The ephemeris file of the objects can be downloaded from `https://kelvins.esa.int/gtoc9-kessler-run/data/`. In Section A the properties of the MRPLP solvers are analyzed in detail using the two carefully selected pairs of objects. In Section B we present the application of the solvers to the full GTOC9 problem. In all simulations the expansion order is fixed to 4, a value that was proved to give a good compromise between accuracy and computational time. An accuracy requirement of 10^{-3} km was used as convergence criterion in all test cases.

A. Illustrative examples

We consider a set of transfers between objects with ID 115 and 70, and object 115 and 82 in the time windows [23765, 23786] MJD2000. These two objects and the reference time window are selected such that the solutions of the MRLP provide poor first guesses for the MRPLP. We have analyzed four transfers with increasing time-of-flight between objects 115 and 70 (labeled A, B, C, and D) and four between objects 115 and 82 (labeled E, F, G, and H). Figure 2 reports the values of Ω for the selected objects in the range of dates of interest, whereas in Tables 1, 2 and 3 the initial and final states are provided for all the tested transfers. As can be seen from the last two columns of Table 2, when the transfer time is approximately 20 days (Case D) the initial and final Ω are almost the same. This results in low Δv in the Keplerian dynamics but high Δv in the perturbed dynamics. On the other hand, Table 3 shows that the difference in Ω for a transfer between object 115 and 82 increases significantly with increasing transfer time. This results in a progressive increase of the Δv in Keplerian dynamics, while the Δv remains almost the same in the perturbed dynamics, due to the natural precession of Ω.

For each test case the minimum and maximum number of revolutions compatible with a minimum perigee radius of 6,600 km and a maximum apogee of 8,600 km are computed (referred as practical solution in the remainder of the section), following the procedure presented in [9]. For each number of revolutions the two solutions of the MRLP are computed and used as first guesses for both the J_2-homotopy and the J_2-map solver.

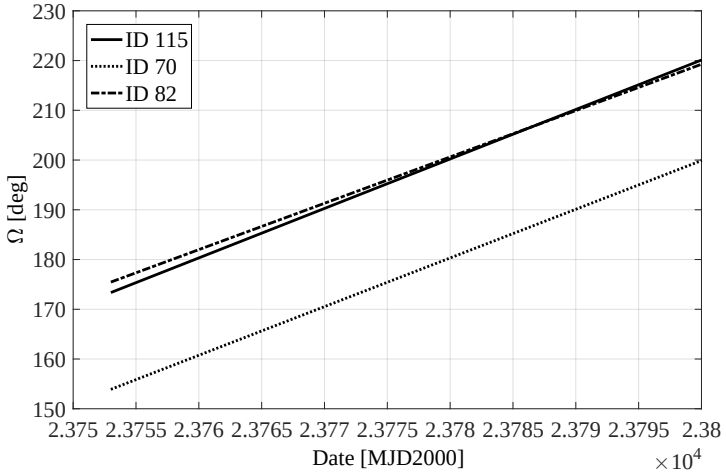

Fig. 2 Evolution of Ω for the selected objects in the range of epochs considered for the test cases.

Table 1 Constant orbital elements of three test objects.

Object ID	70	82	115
a, km	7048.023	7166.722	7128.573
e	$9.301 \cdot 10^{-3}$	$7.285 \cdot 10^{-3}$	$6.938 \cdot 10^{-3}$
i, deg	98.006	98.082	98.472

Table 2 Initial and final states for 115-70 transfer test cases.

	Case A		Case B		Case C		Case D	
ID	115	70	115	70	115	70	115	70
t, MJD2000	23780.527	23785.883	23775.392	23785.614	23770.291	23785.547	23765.018	23785.547
Ω, deg	200.739	186.077	195.631	185.812	190.558	185.748	185.314	185.614
ω, deg	297.386	75.459	312.840	76.315	328.188	76.526	344.054	76.957
ϑ, deg	316.5361	208.913	287.223	223.015	81.602	232.730	60.639	234.096

Table 3 Initial and final states for 115-82 transfer test cases

	Case E		Case F		Case G		Case H	
ID	115	82	115	82	115	82	115	82
t, MJD2000	23780.603	23786.003	23775.889	23786.143	23770.968	23785.654	23765.641	23785.376
Ω, deg	200.814	206.217	196.126	206.348	191.232	205.891	185.934	205.632
ω, deg	297.160	232.214	311.344	231.796	326.151	233.258	342.179	234.087
ϑ, deg	346.871	299.787	348.700	301.754	356.700	299.240	56.760	308.0183

Figure 3 shows the performance of the two algorithms for test cases A, B, C, and D. For each number of revolution only the solution with minimum Δv is reported and the solution is marked as feasible only if the transfer satisfies the constraints on minimum perigee and maximum apogee. It can be noticed that both the J_2-homotopy and J_2-map solvers converge to a solution for any given Keplerian guess. However, the difference in Δv of the Keplerian and perturbed solutions for the same number of revolutions increases with increasing time-of-flight and some practical Keplerian solutions turn into unpractical solutions (highlighted in red in the figures) when J_2 is considered. As expected the transfer Δv is significantly higher when J_2 is included, and the Keplerian Δv becomes very small for a transfer time close to 20 days, as this correspond to a situation in which the departing and arrival state have a similar Ω. It is worth noting that the number of revolutions that corresponds to the minimum Δv is different for Keplerian and perturbed model. There is thus no a priori best Keplerian guess. In general the J_2-homotopy method converges in a lower number of iterations. Besides, in Figure 3 a blue square indicates a solution that is obtained using the velocity of the departing body, $\boldsymbol{v}_1$, as first guess. Note that this initial condition can be used only with the J_2-map solver (the J_2-homotopy requires a Keplerian solution as guess) and typically converges in less iterations compared to using Keplerian guesses. This shows that a Keplerian solution is not required to solve the MRPLP when the number of revolutions is not prescribed. In this case, the obtained solution does not correspond to the minimum Δv, but is not far from it.

Figure 4 shows the performance of the solvers for test cases E, F, G, and H. In contract with the previous test case, the Keplerian solution always overestimates the required Δv as it does not take advantage of the precession of Ω due to J_2. The problem becomes significantly more difficult with increasing transfer time, as the first guesses provided by the MRPL get worse. This is reflected by a significant increase in the number of iterations required for reaching convergence, as well as the appearance of more unpractical solutions. The J_2-homotopy method still converges in less iterations, however, it is worth nothing that in case G this method converges to solutions with very high Δv. In addition, in case G, the J_2-homotopy method fails to converge (either stalls or produce an error in J_2 analytical routine) when the number of revolution is greater than 284. While in both methods there is currently no mean to avoid converging to a non-optimal solution, the J_2-map solver proved to be more robust, because it tends to apply smaller corrections to the velocity. This is probably due to the fact that the J_2-map solver does not use high order map inversion. For test cases A, B, C and D using the velocity of the departing body as first guess showed to reduce the number of iterations significantly. This is also the case for test cases E, F, G, and H and, besides, it results here in finding the minimum Δv solution.

Regarding computation time, one iteration of the J_2-homotopy method takes on average 7.5 ms on a iMac Air with a 2.8 GHz Intel Core i5 processor and 16 GB memory. One iteration of the J_2-map method takes on average 13 ms on the same machine. The higher computational cost of the J_2-map method is due to the multiple polynomial evaluations required in *fsolve* [26], which are carried out in MATLAB by evaluating the maps produced by DACE (the optimized implementation of polynomial evaluation in DACE takes 2 orders of magnitude less).

Figure 5 shows, for all test cases, the path for the continuation parameter ϵ for the minimum Δv transfers. The path is computed automatically by the algorithm by selecting the value of ϵ for which the estimated truncation error of the Taylor map (13) is less than 10^{-6} km/s. From this figure we can conclude that: 1) transfers with shorter durations require less homotopy steps; 2) transfers between ID 115 and 82 are more difficult to solve; and 3) due to the use of high order expansions the number of homotopy steps is limited even for transfers with more than one hundred revolutions.

Both the J_2-homotopy and J_2-map solvers are based on an analytical approximation of the J_2 problem. If the computed solutions are numerically propagated in the full dynamical model given by Eq. (1), the resulting residuals do not meet the accuracy requirements (i.e. errors below 10^{-3} km). The violations of the final position constraints are reported in the third column of Tables 4 and 5, in which only the data corresponding to the minimum Δv solutions are reported. As expected, the residuals tend to increase with the time-of-flight, but remain limited to few kilometers. The application of the iteration-less refinement produces changes in the initial velocity of only a few m/s. This refinement is sufficient to reduce the residuals well below the required tolerance even for the longest transfers.

Figure 6 shows the profile of the primer vector magnitude for the minimum Δv solutions of test cases A and E. The values are obtained with the procedure described in Section IVD using the full dynamics given by Eq. (1) and by exploiting DA tools to compute the state transition matrix. In both cases the transfer is not optimal according to primer vector theory and one or even two corrective maneuvers per orbit could be applied to reduce the transfer Δv.

The analysis is concluded by showing how the expansion of the solution of the MRPLP can be used to find the solution manifold for perturbed initial and final conditions. As an example, assume that the initial or final position, $\boldsymbol{r}_i$ or $\boldsymbol{r}_f$, is perturbed in radial direction (the direction of maximum increase of residuals). Figure 7 shows the residuals of the final state $\Delta \boldsymbol{r}_2$ against the magnitude of the radial perturbation in $\boldsymbol{r}_i$ or $\boldsymbol{r}_f$, for test case A and B, before and after applying a correction using the Taylor expansion. It can be appreciated how a 4-th order Taylor expansion of the MRPLP solution enables the correction of kilometer-level radial perturbations in the initial state and for perturbations of tens of

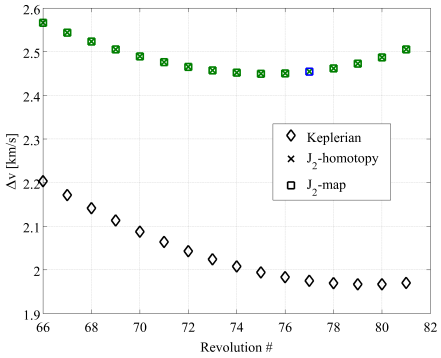

(a) Case A: Δv

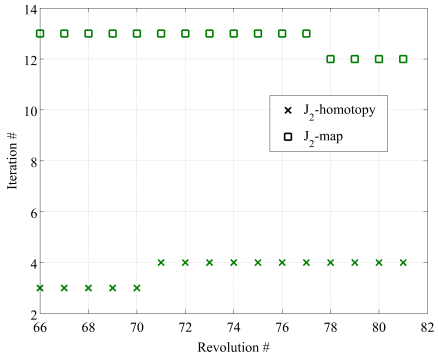

(b) Case A: number of iterations

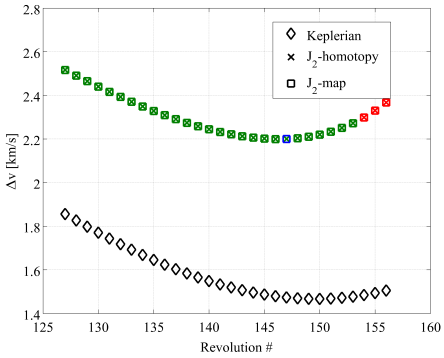

(c) Case B: Δv

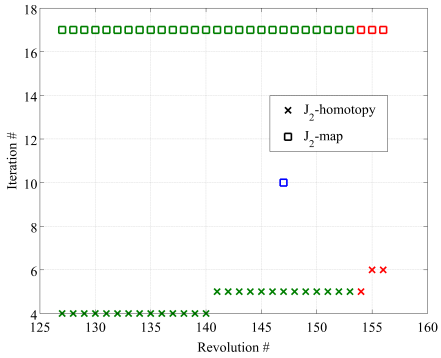

(d) Case B: number of iterations

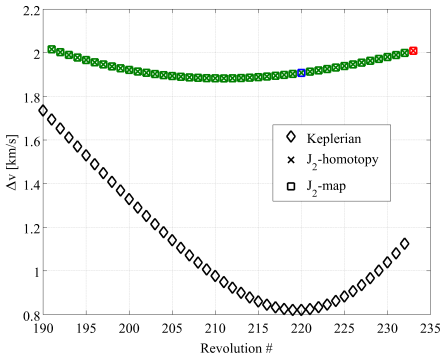

(e) Case C: Δv

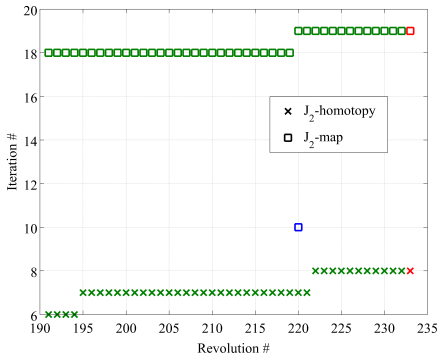

(f) Case C: number of iterations

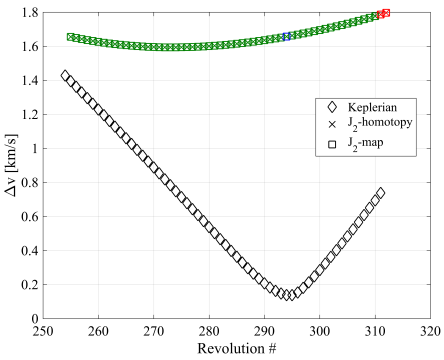

(g) Case D: Δv

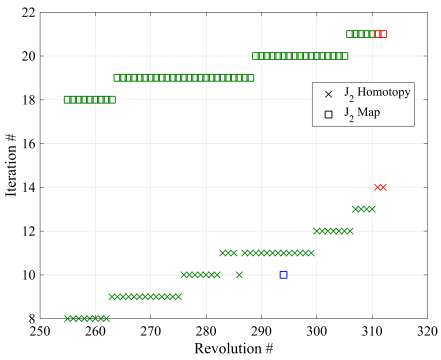

(h) Case D: number of iterations

Fig. 3 Analysis of Δv and convergence for the 115-70 transfer with long time-of-flights. Black indicates the Keplerian solutions, red practical solutions, red unpractical solutions, and blue the solution obtained using v_1 as first guess.

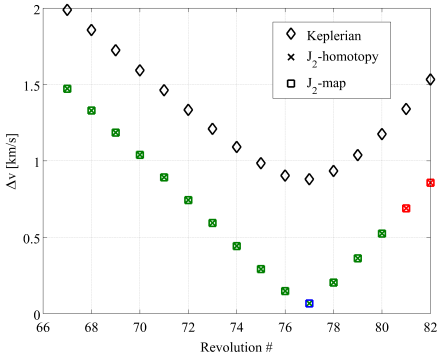

(a) Case E: Δv

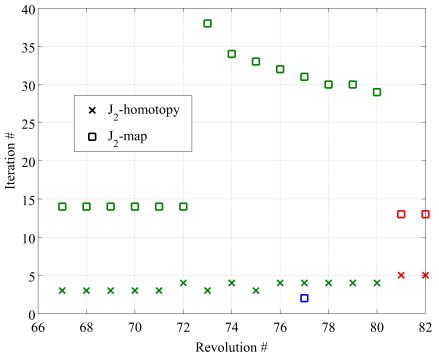

(b) Case E: number of iterations

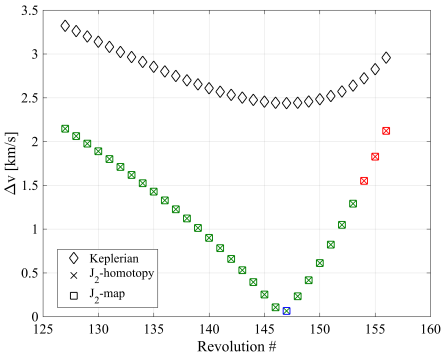

(c) Case F: Δv

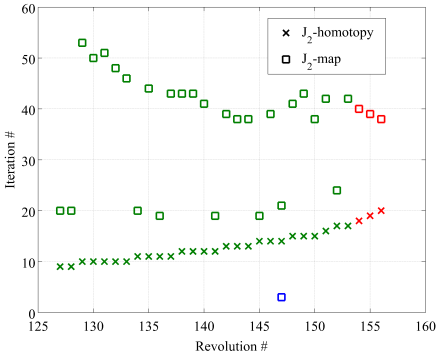

(d) Case F: number of iterations

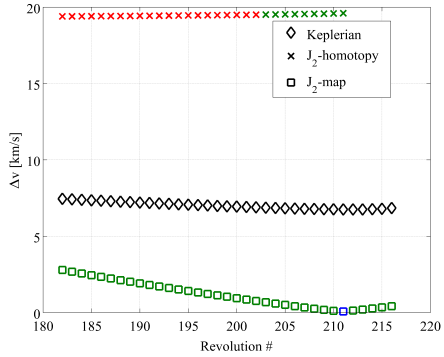

(e) Case G: Δv

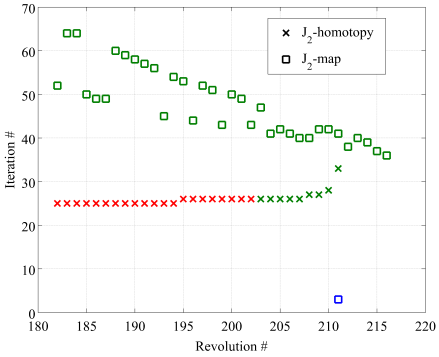

(f) Case G: number of iterations

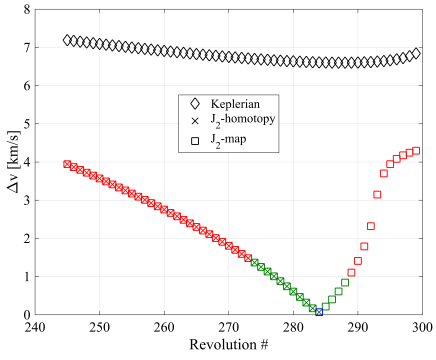

(g) Case H: Δv

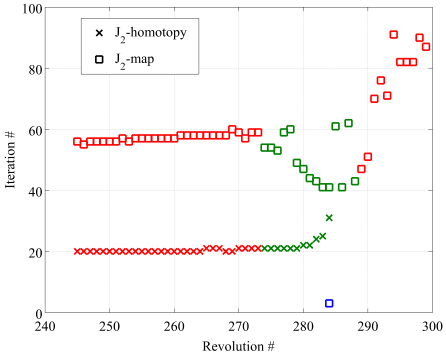

(h) Case H: number of iterations

Fig. 4 Analysis of Δv and convergence for the 115-82 transfer with long time-of-flights. Black indicates Keplerian solution, green solutions that do not violate constraints, red solutions that violate constraints, and blue the solution obtained using the velocity of the departing body as first guess.

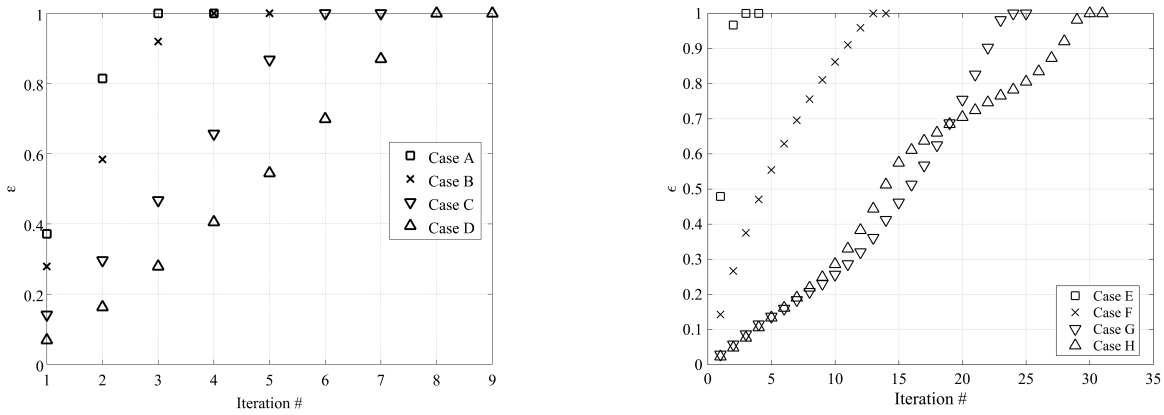

(a) (b)

Fig. 5 Profile of the continuation parameter ϵ for solutions with minimum Δv.

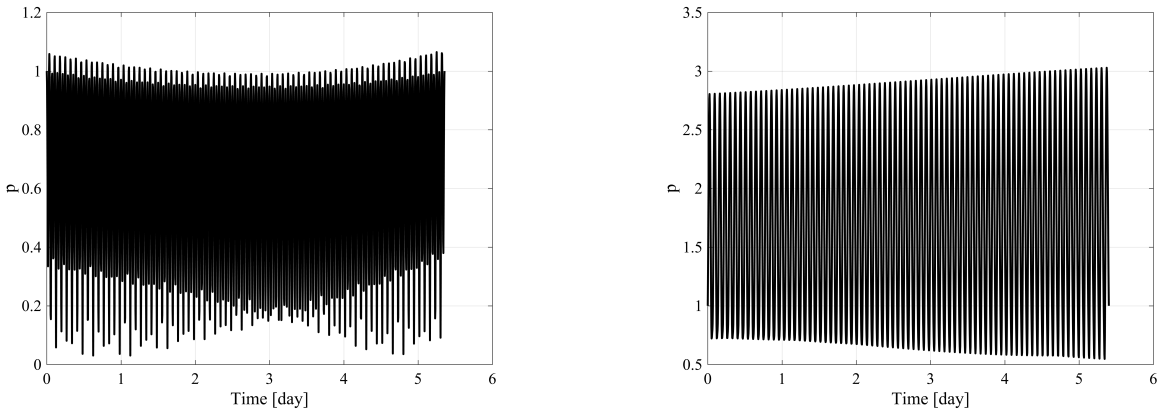

(a) Case A (b) Case E

Fig. 6 Primer vector analysis for minimum Δv transfers.

Table 4 Initial and final Δv and residuals for the 115–70 transfer. For each test case the analysis is presented only for the minimum Δv solution. The residuals are always computed numerically in the $J_2 - J_4$ dynamical model.

	Analytic J_2			Numeric $J_2 - J_4$		
	$\Delta \boldsymbol{v}_1$, km/s	$\Delta \boldsymbol{v}_2$, km/s	$\Delta \boldsymbol{r}_2$, km	$\Delta \boldsymbol{v}_1$, km/s	$\Delta \boldsymbol{v}_2$, km/s	$\Delta \boldsymbol{r}_2$, km
	-0.43152	-0.092073	-3.3396	-0.43174	-0.091666	1.8591e-08
Case A	1.1901	1.1735	-0.55186	1.1896	1.1731	4.4058e-09
	-0.089429	-0.090098	0.075104	-0.088339	-0.088984	-5.0359e-09
	-0.28496	-0.071646	-7.5611	-0.28642	-0.070025	4.3247e-08
Case B	1.1089	1.0488	-0.75067	1.1081	1.0485	8.0208e-09
	-0.067889	-0.054695	0.82595	-0.065169	-0.051981	-2.4995e-08
	0.10565	-0.026461	-8.0559	0.10094	-0.022159	2.0567e-07
Case C	-0.93386	0.881	-0.13239	-0.93305	0.88126	2.8416e-08
	0.27993	-0.19181	-0.293	0.28499	-0.18673	-1.7489e-07
	0.035752	0.067047	6.0311	0.026843	0.074857	3.0323e-05
Case D	-0.74116	0.74319	2.0251	-0.73966	0.74408	3.2122e-06
	0.33722	-0.22163	-14.732	0.34533	-0.21282	-2.7166e-05

Table 5 Initial and final Δv and residuals for the 115–82 transfer. For each test case the analysis is presented only for the minimum Δv solution. The residuals are always computed numerically in the $J_2 - J_4$ dynamical model.

	Analytic J_2			Numeric $J_2 - J_4$		
	$\Delta \boldsymbol{v}_1$, km/s	$\Delta \boldsymbol{v}_2$, km/s	$\Delta \boldsymbol{r}_2$, km	$\Delta \boldsymbol{v}_1$, km/s	$\Delta \boldsymbol{v}_2$, km/s	$\Delta \boldsymbol{r}_2$, km
	-0.00049635	-0.047885	-1.02	0.0007802	-0.047807	-1.3797e-09
Case E	-0.0012413	0.029021	-2.6141	-0.0031303	0.028366	4.8158e-10
	-0.0052617	-0.022797	0.151884	-0.002805	-0.022729	7.1183e-09
	-0.00054946	-0.050597	-1.4939	0.00606572	-0.047679	6.2056e-08
Case F	-0.0013531	0.027112	-5.1336	-0.016835	0.018869	-3.0562e-08
	-0.0030748	-0.024424	-1.8389	0.002966	-0.023248	-3.7517e-07
	-0.0001423	-0.054495	0.61365	0.0030542	-0.059493	-3.0779e-07
Case G	0.00073887	0.026622	-8.3532	0.0084725	0.029879	1.2764e-07
	0.0014842	-0.027431	-16.94	0.0040066	-0.028592	1.6626e-06
	-0.0035206	-0.048783	-3.1678	0.0093124	-0.0675	-2.0184e-05
Case H	0.0035975	0.03253	-5.8682	0.0065088	0.026355	9.6127e-05
	0.0023544	-0.022155	21.657	-0.0085436	-0.021774	0.00063748

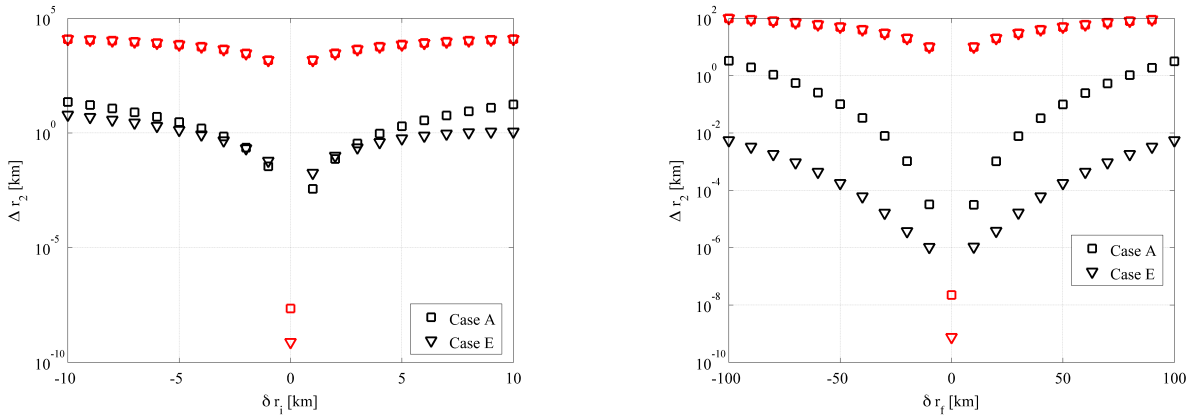

(a) Perturbation on $\boldsymbol{r}_1$

(b) Perturbation on $\boldsymbol{r}_2$

Fig. 7 Use of the expansion of the solution of the MRPLP to correct perturbation in initial and final position vectors. Residuals after correction are reported in black and residuals before correction in red.

kilometers for the final state. It is worth noting that this result is achieved for a time-of-flight longer than 5 days (more than 70 revolutions), which is significantly larger than the time between corrective maneuvers suggested by primer vector theory. Therefore, the proposed approach will be suitable to study the optimal insertion of corrective maneuvers for long-duration rendezvous maneuvers. Besides, the availability of high order expansions of the solution of MRPLP could be profitably used in space situational awareness to study the linkage of radar observations, as already suggested in [10]. Note that the expansion order can be tuned based on accuracy requirements, using as input the estimation of the truncation error.

B. GTOC 9

The goal of GTOC9 was to design N missions to cumulatively remove 123 orbiting debris. A single mission consists of a multiple-rendezvous spacecraft trajectory where a subset of size K of the 123 objects is removed by the delivery and activation of K de-orbit packages. Each spacecraft initial mass m_0 is the sum of its dry mass, the weights of the $K \geq 1$ de-orbit packages, and the propellant mass: $m_0 = m_{dry} + Km_{de} + m_p$. All spacecraft have a dry mass of $m_{dry} = 2000$ kg and a maximum initial propellant mass of $m_p = 5000$ kg. Each de-orbit package has a weight of $m_{de} = 30$ kg.

The n-th mission's starting epoch is denoted with t_s^n and its end epoch with t_f^n . A mission starts with a launch delivering, at t_s^n, one spacecraft at a chosen debris and ends when all the K de-orbit packages on-board have been delivered and activated. An orbiting debris is removed if: a) its position and velocity at some epoch t coincides with the spacecraft position and velocity vector and b) for the following $t_w \geq 5$ days the spacecraft stays in proximity of the debris while delivering and activating a de-orbit package.

The following additional constraints were imposed:

1) the overall time between two successive debris rendezvous, within the same mission, must not exceed 30 days;
2) a time of at least 30 days must be accounted for between any two missions;
3) all mission events must take place in an allowed window, $23467 \leq t \leq 26419$ MJD2000.
4) at no time the orbital pericenter r_p can be smaller than 6,600 km.

The transfers are accomplished with impulsive maneuvers and up to five (deep space) maneuvers can be applied during a single transfer. The objective function to be minimized was

$$J = \sum_{n=1}^{N} \left[c^n + \alpha (m_0^n - m_{dry})^2 \right] \tag{31}$$

in which c^n increased linearly during the competition, as follows:

$$c^n = c_m + \frac{t^n_{submission} - t_{start}}{t_{end} - t_{start}} (c_M - c_m) \tag{32}$$

where $t_{submission}$ is the epoch at which the n-th mission is validated and t_{start} and t_{end} are the start and end dates of the GTOC9 competition. The minimal basic cost c_m is 45 M€, while the maximum cost c_M is 55 M€.

The GTOC9 problem was a complex combinatorial coupled problem with trajectory optimization. The *Mission Learners* team's approach to the problem's solution can be outlined as:

1) for all space debris find the so-called encounter time windows in which their difference in Ω is smaller than a threshold within the full time window of interest;
2) use a multi-objective particle swarm optimizer (PSO) [28] to find the longest missions with minimum rough estimate of mission Δv and compatible with encountering constraints (minor violations allowed at this step);
3) use the same multi-objective PSO to combine missions to meet time constraints, while maximizing the total number of debris removed and minimizing both the number of missions and a rough estimate of the total Δv;
4) refine the encounter dates such that they are compatible with time constraints between transfers and that the difference in RAAN between objects at encounter is minimized;
5) locally optimize each mission Δv using the MRPLP solver;
6) re-optimize the problem to allocate remaining debris and re-distribute them to further reduce the objective function value.

In this section the details of step 5 are given, in particular highlighting how the use of the J_2-map solver combined with splitting the large optimization problem into a sequence of two-dimensional ones allowed the team to achieve a good ranking using a single iMac computer.

The output of steps 1)-4) is a set of preliminary missions, each one defined by a sequence of K space debris to be visited and guesses for the rendezvous times $t^k_{r,g}$, with $k = 1, \ldots, K-1$. No information on transfer times is available at this stage. The object IDs of the space debris for each of the 14 missions that are part of our GTOC9 solution are reported in Table 6. In step 5 accurate Δv, rendezvous epochs, and transfer times are computed. The mission optimization problem is split into a sequence of $K-1$ subproblems with time-of-flight Δt^k and rendezvous times t^k_r as optimization variables. For each subproblem the objective function is given by the transfer Δv,

$$J = ||\boldsymbol{v}_i - \boldsymbol{v}_1|| + ||\boldsymbol{v}_2 - \boldsymbol{v}_f||, \tag{33}$$

which can evaluated by

1) computing, for given t^k_r and Δt^k, the initial state $(\boldsymbol{r}_1(t^k_r - \Delta t^k), \boldsymbol{v}_1(t^k_r - \Delta t^k))$ and final state $(\boldsymbol{r}_2(t^k_r), \boldsymbol{v}_2(t^k_r))$;
2) solving the MRPLP defined by $\boldsymbol{r}_1$, $\boldsymbol{r}_2$ and Δt^k, using the J_2-map method with $\boldsymbol{v}_1$ as first guess for the departing velocity.

The search space of the optimization problem is defined by

$$\begin{aligned} &t^k_{r,g} - t_l \leq t^k_r <\leq t^k_{r,g} + t_l \\ &\Delta t_{min} \leq \Delta t^k \leq \min(t^k_{r,g} - t_l - (t^{k-1}_{r,*} + t_w), \Delta t_{max}), \end{aligned} \tag{34}$$

in which $\Delta t_{min} = 10^{-2}$ day and $\Delta t_{max} = 25$ days are the minimum and maximum time-of-flight, $t^{k-1}_{r,*}$ is the optimal rendezvous time calculated for the previous optimized transfer (when $k = 1$ this coincides with mission start epoch), and t_l defines the search window around the first guess values of the rendezvous dates (a value of 1 day was considered). A PSO optimizer (80 generation and 60 samples) is used to optimize each subproblem. Once a subproblem is solved the transfer is refined in the full J_2 dynamics using the iteration-less refinement. Table 6 reports the start and end epoch, and the start mass for each mission. Note that the evaluation of the objective function (31) results in a total mission cost of 935.8 M€if submitted at the end of the GTOC9 submission period. This value is actually better than the official score by the team, 964.5 M€, due to a bug found in the definition of upper bound of the time-of-flight. It is worth mentioning that the Jet Propulsion Laboratory won the competition by submitting 10 missions and a cost of 731.27 M€.

Tables 7 to 9 report the details of the rendezvous times, transfer times, and Δv to enable the interested reader to make comparisons. Figure 8 shows that the average transfer Δv was in all cases below 537 m/s, but two missions were characterized by transfer Δv greater than 1 km/s. The lowest Δv found for a transfer was 40.1 m/s. Transfer times range from 0.18 to 24.4 days. Transfers with more than 100 revolutions were very frequent, showing that the implementation of efficient MRPLP solvers was of key importance to achieve a good result with limited computational resources. Finally note that to keep the problem simple, our solution method did not consider the inclusion of deep space maneuvers.

VI. Conclusions

Two new solvers for perturbed Lambert problems with several hundreds revolutions were presented. The first solver employs a high order homotopy strategy on the J_2 perturbation, where the homotopy path is automatically computed

Table 6 Overview of missions; epochs, removed objects and start mass per mission.

Mission	Start Epoch [MJD2000]	End Epoch [MJD2000]	Number of objects	Debris Removal Sequence [ID]	Start Mass [kg]
1	23512.10	23581.30	7	118, 22, 46, 114, 38, 97, 105	5287.81
2	23761.92	24043.83	16	115, 82, 11, 71, 45, 43, 26, 109, 7, 85, 47, 39, 21, 2, 63, 70	4962.59
3	24140.83	24319.87	9	84, 86, 103, 121, 16, 74, 92, 49, 23	3734.95
4	24387.72	24456.43	7	108, 44, 104, 120, 37, 75, 18	3671.37
5	24494.71	24641.69	9	79, 50, 56, 42, 107, 111, 58, 91, 78	5353.34
6	24710.64	24902.72	14	69, 14, 100, 106, 95, 30, 33, 93, 55, 28, 77, 9, 94, 90	4724.59
7	24944.31	24969.65	3	83, 88, 64	2866.16
8	25004.29	25221.75	15	67, 51, 99, 1, 36, 31, 122, 40, 102, 89, 35, 62, 54, 0, 4	5423.04
9	25254.49	25308.89	7	52, 41, 24, 32, 119, 117, 72	3878.43
10	25355.85	25484.56	10	112, 8, 15, 87, 27, 20, 59, 61, 98, 116	4315.93
11	25708.49	25890.77	9	80, 12, 3, 68, 60, 17, 53, 57, 5	4771.83
12	25937.20	26060.55	8	110, 65, 10, 81, 6, 96, 73, 48	4482.91
13	26093.47	26115.58	3	76, 66, 113	2782.04
14	26298.15	26418.40	6	101, 34, 19, 29, 25, 13	3745.25

Table 7 Missions rendezvous times

Mission	Rendezvous duration [days]
1	5.00, 6.00, 7.63, 7.07, 6.52, 5.72, 5.00
2	5.00, 6.27, 13.08, 17.18, 17.55, 8.41, 18.69, 24.15, 7.56, 5.26, 14.81, 5.19, 5.84, 18.72, 12.19, 5.00
3	5.00, 5.34, 28.31, 5.88, 10.83, 9.68, 5.02, 16.76, 5.00
4	5.00, 13.17, 5.89, 12.04, 5.64, 5.26, 5.00
5	5.00, 5.63, 5.79, 5.47, 17.11, 5.20, 5.23, 22.56, 5.00
6	5.00, 14.81, 5.58, 6.88, 16.07, 20.71, 5.25, 9.11, 5.47, 12.62, 6.69, 5.68, 22.61, 5.00
7	5.00, 5.18, 5.00
8	5.00, 6.07, 6.55, 6.84, 20.59, 5.09, 10.10, 14.50, 15.56, 6.04, 6.97, 23.39, 6.22, 6.50, 5.00
9	5.00, 5.66, 5.97, 5.70, 5.05, 11.79, 5.00
10	5.00, 5.07, 14.11, 20.27, 9.24, 6.75, 5.67, 6.41, 22.79, 5.00
11	5.00, 5.49, 18.32, 6.00, 5.57, 11.82, 21.34, 5.61, 5.00
12	5.00, 5.55, 6.03, 5.62, 6.85, 27.31, 28.12, 5.00
13	5.00, 5.10, 5.00
14	5.00, 5.74, 5.74, 6.05, 5.21, 5.00

Table 8 Missions transfer times

Mission	Transfer duration [days]
1	12.86, 10.30, 1.12, 0.44, 0.95, 0.59
2	20.00, 4.41, 0.59, 3.50, 4.50, 8.68, 8.97, 3.96, 20.16, 6.95, 4.22, 1.61, 1.52, 2.23, 5.71
3	2.54, 20.82, 0.58, 22.04, 17.82, 4.86, 6.51, 12.05
4	1.77, 3.46, 3.45, 3.00, 2.26, 2.77
5	5.96, 1.38, 13.33, 1.92, 11.05, 7.50, 22.98, 5.89
6	2.92, 0.80, 1.29, 0.31, 2.11, 3.40, 1.07, 1.63, 15.84, 1.18, 17.43, 2.02, 0.60
7	9.41, 0.75
8	2.81, 2.50, 2.51, 18.17, 1.50, 1.14, 18.70, 0.66, 1.29, 0.78, 11.65, 0.54, 7.76, 3.04
9	1.69, 2.04, 0.75, 3.39, 1.57, 0.80
10	4.24, 0.55, 10.09, 8.40, 0.18, 0.80, 0.39, 0.73, 3.02
11	24.42, 1.18, 10.03, 1.35, 19.18, 17.23, 2.15, 22.59
12	6.18, 0.75, 1.05, 20.78, 3.09, 1.56, 0.46
13	5.98, 1.03
14	18.92, 22.18, 22.20, 16.00, 8.20

Table 9 Missions Δv

Mission	Δv [m/s]
1	175.7, 208.8, 303.0, 99.1, 2029.4, 221.3
2	61.6, 49.5, 177.9, 168.5, 118.1, 232.2, 146.5, 210.2, 182.7, 40.1, 310.1, 193.9, 471.3, 90.7, 73.1
3	86.3, 183.6, 154.7, 47.4, 430.2, 486.4, 95.2, 276.2
4	274.5, 428.8, 260.7, 274.2, 255.8, 265.9
5	238.9, 658.6, 395.1, 445.2, 88.0, 598.6, 331.6, 232.5
6	98.4, 195.2, 224.8, 240.9, 111.6, 295.9, 325.3, 153.2, 90.3, 142.7, 162.5, 220.2, 133.6
7	630.7, 441.5
8	99.7, 154.8, 56.4, 113.7, 138.5, 279.9, 150.8, 346.7, 366.3, 285.4, 274.3, 78.2, 164.5, 370.8
9	105.9, 194.1, 716.5, 425.6, 342.1, 168.9
10	385.7, 167.9, 311.7, 513.0, 162.8, 145.4, 159.6, 299.8, 53.1
11	451.8, 363.0, 320.6, 263.7, 295.7, 241.4, 257.5, 400.7
12	1132.0, 464.8, 199.6, 169.1, 132.8, 140.1, 139.3
13	792.3, 175.9
14	242.9, 274.3, 641.1, 493.5, 217.7

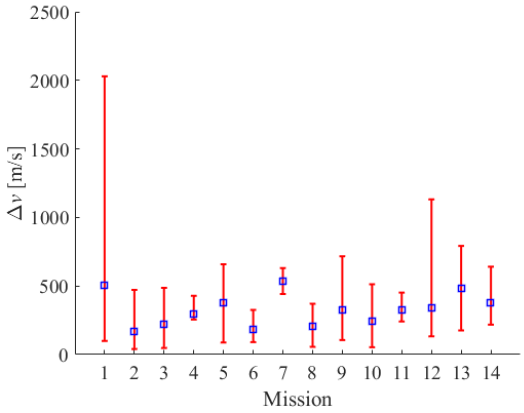

(a) Minimum, maximum and average transfer Δv of each mission.

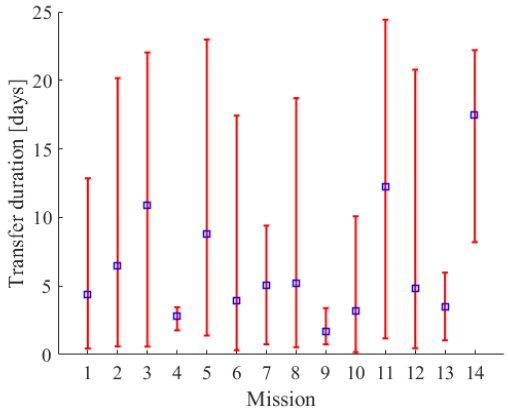

(b) Minimum, maximum and average transfer duration of each mission.

Fig. 8 Analyis of Δv and transfer time

based on an estimation of the truncation error of the Taylor representation of the residuals. Through the test cases it is shown that the J_2-homotopy method converges in few steps when a Keplerian solution is provided. However, convergence to the minimum Δv is not guaranteed. The second approach, the J_2-map solver, is based on repeatedly finding the zeros of a Taylor approximation of the residuals via a standard nonlinear solver. This solver tends to converge in more iterations compared to the J_2-homotopy and typically requires more computational time. However, it has the advantage of not requiring Keplerian solutions as first guesses. This property was exploited to generate optimal transfers for the GTOC9 on an iMac, as illustrated in the test cases section. Both solvers took advantage of high order Taylor expansions and an analytical solution of J_2 problem to reduce the computational time. An iterative-less algorithm to refine J_2 approximated solutions was then presented that enabled meeting stringent accuracy requirements in a full $J_2 - J_4$ dynamical model, even for transfers with more than 200 revolutions.

Finally we have presented a DA-based method to efficiently perform primer vector optimality analyses and to expand the solution of the MRPLP with respect to initial and final uncertainties. These results pave the way towards the implementation of an automatic method to optimally include corrective maneuvers, which will be the focus of future research activity.

Appendix

The expressions for $\{\delta', \mathcal{W}_1\}$, where $\delta' \in (r', \theta', \nu', R', \Theta', N')$ and $\mathcal{W}_1$ is the first-order generating function (corresponding to Eq. (4)), are given by:

$$
\begin{aligned}
\{r', \mathcal{W}_1\} &= R_e^2 \left[\frac{1}{2}\left(3s'^2 - 2\right)\left(\frac{1-\beta'}{2p'} + \frac{\eta' r'}{p'^2} + \frac{\beta'}{2r'}\right) + \frac{s'^2}{4p'}\cos 2\theta' \right] \\
\{\theta', \mathcal{W}_1\} &= \frac{R_e^2}{p'}\left[\frac{R'\left(2(\beta'+5) - 3(\beta'+4)s'^2\right)}{4\Theta'} - \frac{p'\beta' R'\left(3s'^2-2\right)}{4r'\Theta'} - \frac{3\left(5s'^2-4\right)\phi'}{4p'} \right. \\
&\quad \left. + \left(\frac{2-5s'^2}{8p'} - \frac{2-3s'^2}{2r'}\right)\sin 2\theta' + \frac{R'\left(1-2s'^2\right)}{2\Theta'}\cos 2\theta' \right] \\
\{\nu', \mathcal{W}_1\} &= -\frac{R_e^2 c'}{2p'}\left[3\left(\frac{\phi'}{p'} + \frac{R'}{\Theta'}\right) + \left(\frac{1}{2p'} - \frac{2}{r'}\right)\sin 2\theta' + \frac{R'}{\Theta'}\cos 2\theta' \right] \\
\{R', \mathcal{W}_1\} &= \frac{1}{4}R_e^2 R'\left(2 - 3s'^2\right)\left(\frac{\beta'}{r'^2} + \frac{\eta'}{p'^2}\right) - \frac{R_e^2 s'^2 \Theta'}{2p'r'^2}\sin 2\theta' \\
\{\Theta', \mathcal{W}_1\} &= \frac{R_e^2 s'^2}{p'}\left[\Theta'\left(\frac{1}{r'} - \frac{1}{4p'}\right)\cos 2\theta' + \frac{R'}{2}\sin 2\theta' \right] \\
\{N', \mathcal{W}_1\} &= 0
\end{aligned}
$$

where $\beta' = 1/(1+\eta')$ and $p' = \Theta'^2/\mu$.

Acknowledgments

R. Armellin acknowledges the support received by the Marie Sklodowska-Curie grant 627111 (HOPT - Merging Lie perturbation theory and Taylor Differential algebra to address space debris challenges). This work has been partially funded by the Spanish Finance and Competitiveness Ministry under Project ESP2014-57071-R. David Gondelach was funded by Surrey Space Centre of the University of Surrey and an EPSRC Doctoral Training Grant awarded by the University of Southampton. The authors thank all other Mission Learners team members, in particular Cristina Parigini for her contribution in solving the combinatorial part of the GTOC9.

References

[1] Gauss, C. F., and Davis, C. H., *Theory of the motion of the heavenly bodies moving about the sun in conic sections*, Courier Corporation, 2004.

[2] Gooding, R., "A procedure for the solution of Lambert's orbital boundary-value problem," *Celestial Mechanics and Dynamical Astronomy*, Vol. 48, No. 2, 1990, pp. 145–165.

[3] Arora, N., and Russell, R. P., "A fast and robust multiple revolution Lambert algorithm using a cosine transformation," *Paper AAS*, Vol. 13, 2013, p. 728.

[4] Prussing, J. E., "A class of optimal two-impulse rendezvous using multiple-revolution lambert solutions." *Journal of Astronautical Sciences*, Vol. 48, No. 2, 2000, pp. 131–148.

[5] Engels, R., and Junkins, J., "The gravity-perturbed Lambert problem: A KS variation of parameters approach," *Celestial Mechanics and Dynamical Astronomy*, Vol. 24, No. 1, 1981, pp. 3–21.

[6] Bai, X., and Junkins, J. L., "Modified Chebyshev-Picard iteration methods for solution of initial value problems," *The Journal of the Astronautical Sciences*, Vol. 59, No. 1-2, 2012, pp. 327–351.

[7] Woollands, R. M., Younes, A. B., and Junkins, J. L., "New solutions for the perturbed lambert problem using regularization and picard iteration," *Journal of Guidance, Control, and Dynamics*, 2015.

[8] Der, G. J., "The superior Lambert algorithm," *AMOS, Maui, Hawaii*, 2011.

[9] Yang, Z., Luo, Y.-Z., Zhang, J., and Tang, G.-J., "Homotopic perturbed Lambert algorithm for long-duration rendezvous optimization," *Journal of Guidance, Control, and Dynamics*, 2015.

[10] Woollands, R. M., Read, J. L., Probe, A. B., and Junkins, J. L., "Multiple Revolution Solutions for the Perturbed Lambert Problem using the Method of Particular Solutions and Picard Iteration," *The Journal of the Astronautical Sciences*, 2016, pp. 1–18.

[11] Berz, M., *Differential Algebraic Techniques, Entry in Handbook of Accelerator Physics and Engineering*, World Scientific, New York, 1999.

[12] Wittig, A., Di Lizia, P., Armellin, R., Makino, K., Bernelli-Zazzera, F., and Berz, M., "Propagation of large uncertainty sets in orbital dynamics by automatic domain splitting," *Celestial Mechanics and Dynamical Astronomy*, Vol. 122, No. 3, 2015, pp. 239–261. doi:10.1007/s10569-015-9618-3, URL http://dx.doi.org/10.1007/s10569-015-9618-3.

[13] Aksnes, K., "On the use of the hill variables in artificial satellite theory: Brouwer's Theory," *Astronomy and Astrophysics*, Vol. 17, 1972, pp. 70–75.

[14] Jezewski, D. J., "Primer vector theory and applications," *In: Technical report, Lyndon B. Johnson Space Center, NASA*, 1975.

[15] Berz, M., *Differential Algebraic Techniques, Entry in Handbook of Accelerator Physics and Engineering*, World Scientific, New York, 1999a.

[16] Berz, M., *The new method of TPSA algebra for the description of beam dynamics to high orders*, Los Alamos National Laboratory, 1986. Technical Report AT-6:ATN-86-16.

[17] Berz, M., "The method of power series tracking for the mathematical description of beam dynamics," *Nuclear Instruments and Methods A258*, 1987.

[18] Berz, M., *Modern Map Methods in Particle Beam Physics*, Academic Press, 1999b.

[19] Berz, M., and Makino, K., *COSY INFINITY version 9 reference manual*, Michigan State University, East Lansing, MI 48824, 2006. MSU Report MSUHEP060803.

[20] Rasotto, M., Morselli, A., Wittig, A., Massari, M., Di Lizia, P., Armellin, R., Valles, C., and Ortega, G., "Differential Algebra Space Toolbox for Nonlinear Uncertainty Propagation in Space Dynamics," *6th International Conference on Astrodynamics Tools and Techniques, ICATT 2016. Proceedings of the*, 2016, pp. 1–11.

[21] Di Lizia, P., Armellin, R., and Lavagna, M., "Application of high order expansions of two-point boundary value problems to astrodynamics," *Celestial Mechanics and Dynamical Astronomy*, Vol. 102, No. 4, 2008, pp. 355–375.

[22] Valli, M., Armellin, R., Di Lizia, P., and Lavagna, M., "Nonlinear mapping of uncertainties in celestial mechanics," *Journal of Guidance, Control, and Dynamics*, Vol. 36, No. 1, 2012, pp. 48–63.

[23] San-Juan, J. F., López, L. M., and López, R., "MathATESAT: A symbolic-numeric environment in Astrodynamics and Celestial Mechanics," *Lecture Notes in Computer Science*, Vol. 6783, No. 2, 2011, pp. 436–449. doi:10.1007/978-3-642-21887-3_34.

[24] Deprit, A., "Delaunay normalisations," *Celestial Mechanics and Dynamical Astronomy*, Vol. 26, No. 1, 1982, pp. 9–21.

[25] Lara, M., "Efficient Formulation of the Periodic Corrections in Brouwer's Gravity Solution," *Mathematical Problems in Engineering*, Vol. 2015, No. Article ID 980652, 2015, p. 9. doi:10.1155/2015/980652.

[26] MATLAB and Optimization Toolbox , *Release 2014a*, The MathWorks Inc., Natick, Massachusetts, 2014.

[27] Lawden, D. F., *Optimal trajectories for space navigation*, Butterworths, 1963.

[28] Armellin, R., San-Juan, J. F., and Lara, M., "End-of-life disposal of high elliptical orbit missions: The case of INTEGRAL," *Advances in Space Research*, Vol. 56, No. 3, 2015, pp. 479–493.